AIAA JOURNAL
Vol. 40, No. 6, June 2002

Wavelet Multiresolution Analysis of Stereoscopic Particle-Image-Velocimetry Measurements in Lobed Jet

Hui Li*
Kagoshima University, Kagoshima 890-0065, Japan
Hui Hu†
Michigan State University, East Lansing, Michigan 48824
and
Toshio Kobayashi,‡ Tetsuo Saga,§ and Nobuyuki Taniguchi¶
University of Tokyo, Tokyo 153-8505, Japan

A wavelet-based vector multiresolution technique was developed and applied to a high-resolution stereoscopic particle image velocimetry system for studying the three-dimensional multiscale structure features of the lobed jet mixing flow. The instantaneous three-dimensional velocity vectors were successfully decomposed into large- and small-scale velocity fields, and existence of very strong multiscale turbulent structures were confirmed in the near field of the lobed jet. Within the central scale range of 16 mm, the instantaneous pairs of large-scale streamwise and horseshoe vortices can be clearly observed around the lobe peak regions and lobe troughs, respectively, and begin to breakdown and spread outward at downstream. The stronger small-scale streamwise vortices were found in the lobe regions, which first spread outward along the lobes and then develop to the whole measured flowfield. These small-scale streamwise vortices also play an important role in the enhance mixing process. The stronger alternate positive and negative peaks of small-scale axial velocity component, which appear at the trailing edge of the lobed nozzle in the near field, indicate the existence of the Kelvin–Helmholtz or normal vortices.

Introduction

THE turbulent jet exhibited complex structures with a wide range of coexisting scales and a variety of shapes in the dynamics, and its physics of mixing process is important in the engineering. It is a well-known fact that the streamwise vortices generated in a jet flow, in addition to the azimuthal (or ring-type) vortices, have been found to mix fluid streams even more efficiently. The distortion of azimuthal vortex structure can lead to streamwise vortices under certain conditions. The streamwise vortices in jet mixing flows can be generated by many methods. One of the methods is to use a lobed nozzle to generate the large-scale streamwise vortices and to induce rapid mixing, which has been considered to be one promising method for the enhanced jet mixing process. More recently, it has become obvious that lobed mixers provide the most mixing enhancement in the presence of a velocity difference or normal vorticity component.

The first application of the lobed mixer was for jet noise reduction and net thrust increase of a turbofan jet engine[1] because of the mixing characteristics of lobed mixers and their advantage over the convectional nozzle designs. Now the lobed mixer has been applied to the combustion chambers in engine, the spread of pollutants at industrial sites and so on, and becomes an extraordinary fluid mechanics device for efficiently mixing two different flow streams in determining the length. Because of these practical applications in engineering, the investigation of the detailed mixing mechanisms becomes significant. Paterson[2] provided the first detailed experimental data in the mixing region downstream of axisymmetric lobed nozzles by using laser Doppler velocimetry (LDV). Originally, it was believed that the mixing enhancement mechanism was solely caused by the increased interfacial area. However, his study found that the flowfield of downstream was dominated by strong secondary flow structures along with relatively large-scale streamwise vortices having scales on the order of the lobe height, which played a major role in the enhanced mixing process. Also, a horseshoe vortex on the order of the lobe half-height was found to exist in the lobe troughs. The contribution of these vortices to the overall mixing process was not clear, but it was believed that these vortices were created by the lobe geometry and the trailing-edge Kutta condition. Most of the later studies concentrated on discovering the underlying physics of the two-dimensional lobed mixing process. Werle et al.[3] found that the vortex formation process was an inviscid effect, and the mixing process took place in three basic steps: the vortices form, intensify, and then rapidly break down into small-scale turbulence. Eckerle et al.[4] studied mixing downstream of a lobed mixer at two velocity ratios using a two-component LDV. It was found that the breakdown of the large-scale vortices and the accompanying increase in turbulent mixing are significant parts of the mixing process. Ukeiley et al.[5,6] applied the proper orthogonal decomposition (POD) to a rake of 15 single-component hot-wire data obtained in a lobed mixer flowfield. They showed that the large-scale vortex, as defined by the POD, breaks down, and the flow becomes more homogeneous. McCormick[7] reported more detailed experimental investigation of the vortical and turbulent structure using the pulsed-laser sheet flow visualization with smoke and three-dimensional velocity measurements taken with a hot wire. Their study confirmed a new vortex structure existing in addition to the well-known streamwise vortex array and found that the streamwise vorticity deforms the normal vortex into a pinched-off structure that might also enhance small-scale turbulent mixing. Recently, the mixing process in a coaxial jet where the inner nozzle is a lobed mixer was experimentally studied by Belovich and colleagues.[8,9] Detailed flow visualization and velocity measurements with LDV were performed, and different mixing mechanisms for each velocity ratio were discussed.

Presented as Paper 2001-0696 at the AIAA 39th Aerospace Sciences Meeting, Reno, NV, 8–11 January 2001; received 5 March 2001; revision received 12 September 2001; accepted for publication 19 October 2001. Copyright © 2002 by the American Institute of Aeronautics and Astronautics, Inc. All rights reserved. Copies of this paper may be made for personal or internal use, on condition that the copier pay the $10.00 per-copy fee to the Copyright Clearance Center, Inc., 222 Rosewood Drive, Danvers, MA 01923; include the code 0001-1452/02 $10.00 in correspondence with the CCC.

*Assistant Professor, Department of Mechanical Engineering, 1-21-40, Korimoto; li@mech.kagoshima-u.ac.jp. Member AIAA.
†Research Associate, Turbulent Mixing and Unsteady Aerodynamics Laboratory.
‡Professor, Institute of Industrial Science, 4-6-1, Komaba, Meguroku.
§Assistant Professor, Institute of Industrial Science, 4-6-1, Komaba, Meguroku.
¶Associate Professor, Institute of Industrial Science, 4-6-1, Komaba, Meguroku.

During the past couple of years, the development of particle image velocimetry (PIV) techniques has made it possible to provide more detailed information on flow structure, such as the instantaneous values of various flow quantities, as well as their distribution and transient variation. Hu et al.[10,11] employed two-dimensional and stereoscopic PIV systems to measure the near flowfield of a lobed jet mixing flow. The characteristics of the mixing process in a lobed jet mixing flow compared with a conventional circular jet flow were discussed. Despite the usefulness of information obtained by examining the measured instantaneous flowfields and the time-mean turbulent quantities, further detail of the mixing process associated with the instantaneous multiscale structures has not yet been clarified.

In the past decade there has been a growing interest in the use of wavelet analysis for turbulent data. This technique can track turbulent structures in terms of time and scale and extracts new information on turbulence structures. The continuous wavelet transform has been proposed to analyze turbulent structures in terms of time and scale by Li and Nozaki[12] and Li.[13] The coefficients of the continuous wavelet transform are known to extract the characterization of local regularity continuously. However, the continuous inverse wavelet transform is unable to reconstruct the original function because the mother wavelet function is a nonorthogonal function. It is important to reconstruct the original signal from wavelet composition in studying multiscale turbulent structures. On the other hand, the discrete wavelet transform allows an orthogonal projection on a minimal number of independent modes and is invertible. Such analysis can produce a multiresolution representation and might be also used to analyze turbulent flows. Charles[14] first used the one-dimensional discrete wavelet transform to obtain local energy spectra and the flux of kinetic energy from experimental and direct numerical simulation data. Staszewski et al.[15] identified the turbulent structures of the atmospheric boundary layer using the discrete wavelet transform. Li et al.[16,17] employed the discrete wavelet transform to evaluate eddy structures of a jet in the dimension of time and scale. Li et al.[18] also applied the two-dimensional orthogonal wavelets to turbulent images and extracted the multiresolution turbulent structures. To identify the turbulent structures in the dimension of time and scale, however, there are no published studies that concern the extraction of multiscale turbulent structures from the PIV measurement vector field. For the highly three-dimensional flowfields like lobed jet mixing flows, the convectional analysis of three-dimensional PIV measurement results cannot reveal the contribution of the multiscale structures to the mixing mechanisms successfully.

The aim of this paper is to apply a new signal processing technique, called vector wavelet multiresolution analysis, to analyze the three-dimensional measurement results of a high-resolution stereoscopic PIV system in the near field for providing a fundamental understanding of the multiscale vortical structures and why vorticity dynamics greatly impact the mixing process of lobed jet.

Two-Dimensional Discrete Vector Wavelet Transform

Here, we consider analyzing a two-dimensional vector field $\boldsymbol{f}(x_1, x_2)$. The simplest way of constructing a two-dimensional orthogonal wavelet basis is to take the simple production of two one-dimensional orthogonal wavelet bases:

$$\Psi_{m;n_1,n_2}(x_1, x_2) = 2^{-m}\psi\left(2^{-m}x_1 - n_1\right)\psi\left(2^{-m}x_2 - n_2\right) \quad (1)$$

where m denotes the dilation index and n_1 and n_2 represent the translation index. The oldest example of a function $\psi(x)$ for which the $\psi_{m,n}(x)$ constitutes an orthogonal basis is the Haar function, constructed long before the term *wavelet* was coined. In the past 10 years various orthogonal wavelet bases have been constructed, for example, Meyer basis, Daubechies basis, Coifman basis, Battle–Lemarie basis, Baylkin basis, and spline basis, etc. They provide excellent localization properties both in physical space and frequency space. In this study we use the Daubechies basis with index $N = 20$, which is not only orthonormal but also has smoothness and compact support, to analyze the vector field.

The two-dimensional discrete vector wavelet transform is defined by

$$\boldsymbol{Wf}_{m;n_1,n_2} = \sum_i \sum_j \boldsymbol{f}\left(x_1^i, x_2^j\right)\Psi_{m;n_1,n_2}\left(x_1^i, x_2^j\right) \quad (2)$$

As in the Fourier series, dilation by larger m compresses the vector field on the x and y axes. Altering n_1 and n_2 has the effect of sliding the vector along the x and y axes, respectively.

The reconstruction of the original vector field can be achieved by

$$\boldsymbol{f}(x_1, x_2) = \sum_m \sum_{n_1} \sum_{n_2} \boldsymbol{Wf}_{m;n_1,n_2}\Psi_{m;n_1,n_2}(x_1, x_2) \quad (3)$$

Vector Wavelet Multiresolution Technique

Wavelet multiresolution analysis was formulated in the fall of 1986 and was applied to image processing in 1989. Since then, researchers have been making widespread use of wavelet multiresolution analysis. The goal of the wavelet multiresolution analysis is to get a representation of a signal or an image that is written in a parsimonious manner as a sum of its essential components. That is, a parsimonious representation of a signal or an image will preserve the interesting features of the original signal or image, but will express the signal or image in terms of a relatively small set of coefficients. It is a well-known fact that the vector field often includes too much information for multiscale vision processing. A multiresolution algorithm can process fewer data by selecting the relevant details that are necessary to perform a particular recognition task. Coarse-to-fine searches process first a low-resolution vector field and then zoom selectively into finer scales information.

In mathematics, the multiresolution analysis consists of a nested set of linear function spaces V_j with the resolution of functions in increasing with j. More precisely, the closed subspaces V_j satisfy

$$\cdots V_2 \subset V_1 \subset V_0 \subset V_{-1} \subset V_{-2} \cdots \quad (4)$$

with

$$\overline{\bigcup_{j \in Z} V_j} = L^2(\Re^2)$$

$$\bigcap_{j \in Z} V_j = \{0\} \quad (5)$$

The basis functions for the subspaces V_j are called scaling functions of the multiresolution analysis. For every $j \in Z$ define the wavelet spaces W_j to be the orthogonal complement of in V_{j-1} of V_j. We have

$$V_{j-1} = V_j \oplus W_j \quad (6)$$

where $\oplus$ represents the orthogonal space sum and

$$W_j \perp W_{j'} \qquad \text{if} \qquad j \neq j' \quad (7)$$

that is, any function in V_{j-1} can be written as the sum of a unique function in V_j and a unique function in W_j. In $L^2(\Re^2)$ the orthogonal basis for W_j is the family of wavelets that is defined. Thus, $L^2(\Re^2)$ can be decomposed into mutually orthogonal subspaces and can be written as

$$L^2(\Re^2) = \bigoplus_{j \in Z} W_j \quad (8)$$

In this study the procedure of the vector wavelet multiresolution analysis can be summarized in two steps:

1) Compute the wavelet coefficients of vector data based on the discrete wavelet transform of Eq. (2).

2) The inverse wavelet transform of Eq. (3) is applied to wavelet coefficients at each wavelet level, and vector components are determined at each level or scale.

Of course, a sum of these essential vector components can recover the original vector field. The vector wavelet multiresolution analysis can perform an extraction of the multiscale structures and decompose the vector field in both Fourier and physical spaces. This technique is unique in terms of its capability to separate turbulence structures of different scales.

Experimental Setup and Stereoscopic PIV System

A test lobed nozzle with six lobes, as shown in Fig. 1, is used in the present study. The width of each lobe is 6 mm, and the height of each lobe is 15 mm ($H = 15$ mm). The inner and outer penetration angles

of the lobed structures are $\theta_{in} = 22$ deg and $\theta_{out} = 14$ deg, respectively. The equivalent nozzle diameter is designed to be $D = 40$ mm. The z axis is taken as the direction of the main stream; the $x-y$ plane is perpendicular to the z axis and is taken as the cross plane of the lobed jet. The velocity components in x, y, and z directions are u, v, and w, respectively.

Figure 2 shows the air jet experimental setup used in the present study. A centrifugal compressor was used to supply airjet flows. A cylindrical plenum chamber with honeycomb structures was used to settle the airflow. Through a convergent connection (convergent ratio is about 50:1) the airflow is exhausted from the test nozzles.

The velocity of the airjet exhausting from the test nozzle can be adjusted, and the core jet velocity U_0 was set at about 20 m/s in the present study. The Reynolds number of the jet flow is about 60,000 based on the equivalent nozzle diameter D and the core jet velocity. A seeding generator, which is composed by an air compressor and several Laskin nozzles, was used to generate 2–3 μm Di-2-EthylHexyl-Sebact droplets as tracer particles in the jet flow. According to Raffel et al.,[19] the time response of $1 \sim 5$ μm oil droplets in an airflow is about 0.0004 s. Therefore, the expected frequency response of the tracer particles used in our experiment is 2500 Hz.

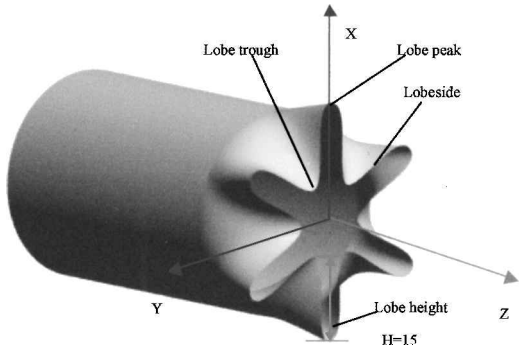

Fig. 1 Test lobed nozzle.

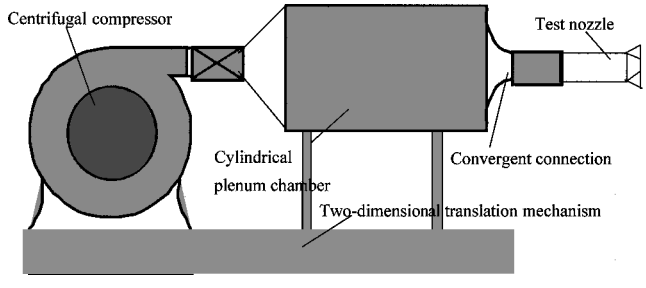

Fig. 2 Airjet experimental setup.

Figure 3 shows the schematic of the stereoscopic PIV system used in the present study. The objective jet mixing flows were illuminated by a double-pulsed Nd:YAG laser set (New Wave 50-mJ/pulse), with the laser sheet thickness being about 2 mm. The double-pulsed Nd:YAG laser set can supply the pulsed laser at the frequency of 15 Hz. The time interval between the two pulsed illuminations was settled as 30 μs. Two high-resolution (1008×1016 pixels) cross-correlation charge-coupled device (CCD) cameras (TSI PIVCAM10-30) were used to do stereoscopic PIV image recording. The two CCD cameras were arranged in an angular displacement configuration to get a big overlapped view. To have the measurement field focused on the image planes perfectly, tilt-axis mounts were installed between the camera bodies and lenses, and the lenses and camera bodies were adjusted to satisfy the Scheimpflug condition. In the present study the distance between the illuminating laser sheet and image recording plane of the CCD camera is about 650 mm, and the angle between the view axes of the two cameras is about 50 deg. For such an arrangement the size of the overlapped view of the two image recording cameras for stereoscopic PIV system is about 80×80 mm.

The two-dimensional particle image displacements in every image planes were calculated separately by using Hierarchical Recursive PIV (HR-PIV) software.[20] The Hierarchical Recursive PIV software is based on a hierarchical recursive process of conventional spatial correlation operation with offsetting of the displacement estimated by the former iteration step and hierarchical reduction of the interrogation window size and search distance in the next iteration step. Because 32×32 pixel windows and 50% overlapping grids were used for the final step of the recursive correlation operation, the spatial resolution of the present stereoscopic PIV measurement is expected to be about $2 \times 2 \times 2$ mm.

According to the comparison of the simultaneous measurement results of our stereoscopic PIV system and a LDV system, the error level of the instantaneous velocity data obtained by the stereoscopic PIV system was less than 2.0%.

Results and Discussion

Instantaneous Three-Dimensional Multiscale Velocity Fields

To gain insight into the multiscale flow structures, vector wavelet multiresolution analysis is applied to the three-dimensional measurement results of PIV. In the present study the measured three velocity components of 64×64 are used. The instantaneous velocity vector $\boldsymbol{u}(x, y)$ is first decomposed into three compositions $\boldsymbol{u}_i(x, y)$ with different wavelet levels or scales, where i represents the scale. Then three velocity vector compositions $\boldsymbol{u}_i(x, y)$ within different scale ranges are produced based on vector wavelet multiresolution analysis. To describe the frequency character of vector component at each wavelet level, the central scales of three velocity vector compositions were determined by Fourier transform. The velocity vector composition of wavelet level 1, which corresponds to the central scale of 16 mm, is employed to describe the large-scale flow

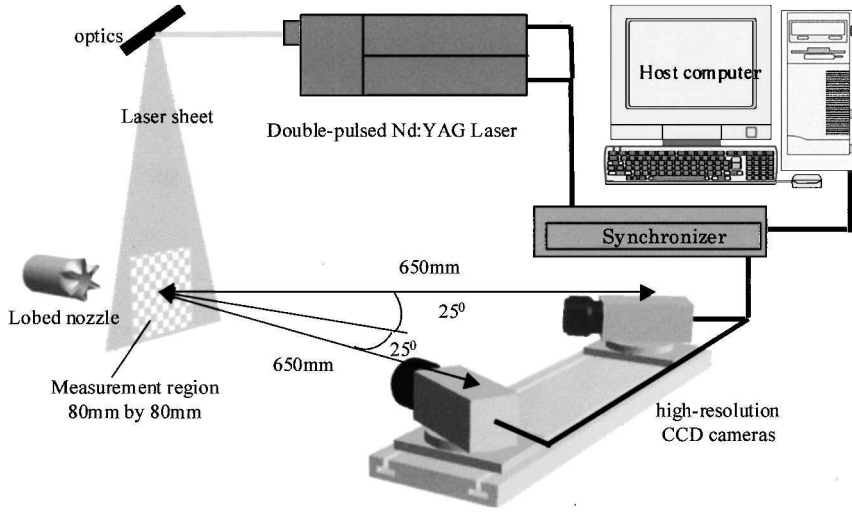

Fig. 3 Schematic of the stereoscopic PIV system.

structure. The sum of velocity vector compositions of wavelet levels 2 and 3, which corresponds to the central scale of 6 mm, constructs the smaller-scale flow structure. Of course, the measured velocity vector $\boldsymbol{u}(x, y)$ can be written as the sum of three velocity vector compositions $\boldsymbol{u}_i(x, y)$, that is,

$$\boldsymbol{u}(x, y) = \sum_{i=1}^{3} \boldsymbol{u}_i(x, y) \tag{9}$$

Figure 4a shows an instantaneous velocity vectors of the stereoscopic PIV measurement in the cross plane [(x, y)-plane view] overlapping on the corresponding the contour of the axial velocity component at a downstream location of $z/D = 0.5$. The monochrome mappings have been assigned to the value of axial velocity component, and the highest concentration is displayed as white and the lowest as a black. These are the original data before the wavelet decomposition. The contour of the axial velocity component exhibits the geometry of the lobed nozzle approximately. Seven well-defined peaks, representing the six lobes and the central core, can be clearly observed. The vector plot shows instantaneous irregular flow structures that imply the multiscale structures. The larger velocity component appears in the lobe regions. The irregular streamwise vortices can be seen to be in the same configuration as the trailing-edge geometry of the lobed nozzle.

The analysis results of the instantaneous velocity vectors of the stereoscopic PIV measurement (Fig. 4a) based on the wavelet vector multiresolution technique are shown in Figs. 4b and 4c, in which the two different scale components of instantaneous velocity field can be seen. It has been verified that the two decomposed instantaneous vector components can be summed to obtain the original vector field of Fig. 4a. It provides a validation for the present data analysis technique. Figure 4b displays the large-scale structures of the original velocity field with a central scale of 16 mm. The contour of the axial velocity component exhibits well-defined geometry of the lobed nozzle. The vector plot shows clearly six pairs of large-scale counter-rotating streamwise vortices around either side of the lobe peaks. This location is the region of the formation and intensification processes of the large-scale streamwise vortices generated by the lobed nozzle around the lobe peak regions. These vortices correspond quite well to the irregular vortices that appear in Fig. 4a. The vector plot also clearly reveals that the cross-stream flow expands, indeed, outward along the lobes, and ambient flow ejects inward in the lobe troughs, which results in the generation of large-scale streamwise vortices. From the velocity vector plot the new vortices can be clearly observed near the lobe troughs, which are also formed as a result of lobed nozzle around the lobe trough regions. They also play a important role in the enhance mixing process. The insignificant differences between Figs. 4a and 4b imply that large-scale structures dominate the flowfield near the nozzle. The flow structures with a central scale of 6 mm are shown in Fig. 4c. The velocity vector indicates the presence of the small-scale streamwise vortices that appeared around the six lobe positions. By comparing Figs. 4b and 4c, one finds that some of these small-scale vortices are contained in the streamwise vortices. The larger velocity vectors can be found in the lobe regions, which enhance the small-scale mixing process. The contour of the axial velocity component indicates that the alternate positive and negative peaks also appear around the edge position of the lobed nozzle within the central scale of 6 mm. It suggests that these peaks imply the existence of the Kelvin–Helmholtz or normal vortices whose axes are inclined or aligned to the streamwise direction because the normal vortex is formed as result of an axial velocity difference and has a small scale at the cross-stream plane. It can be seen that the shape of Kelvin–Helmholtz or normal vortex ring has almost the same geometry as the trailing edge of the lobed nozzle as it is expected. Such structure features cannot be extracted by traditional techniques.

Figure 5a shows the stereoscopic PIV measurement results of the cross plane at $z/D = 1$. From distributions of the instantaneous velocity vector field and contour of axial velocity, the geometry of the lobed nozzle can also be identified. The large-scale structures of the original velocity field with a central scale of 16 mm are shown in Fig. 5b. The vector plot clearly reveals that the streamwise vortices or large-scale structures have spread outward along the lobes. The extent of the vortices is slightly beyond the area over which data

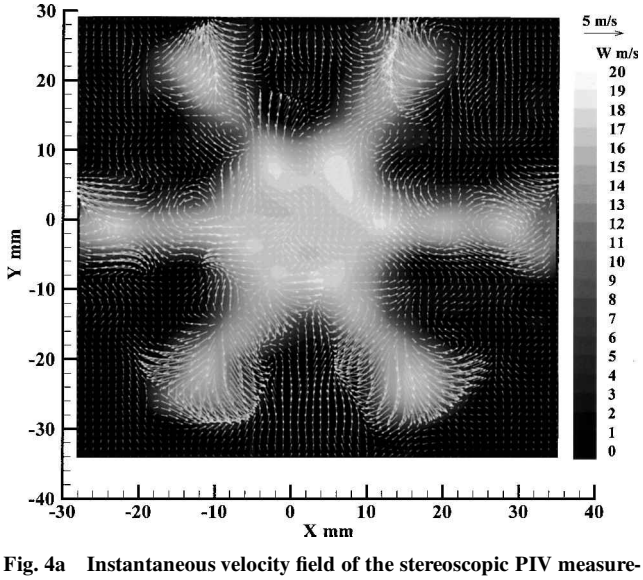

Fig. 4a Instantaneous velocity field of the stereoscopic PIV measurement results in the cross plane of $z/D = 0.5$.

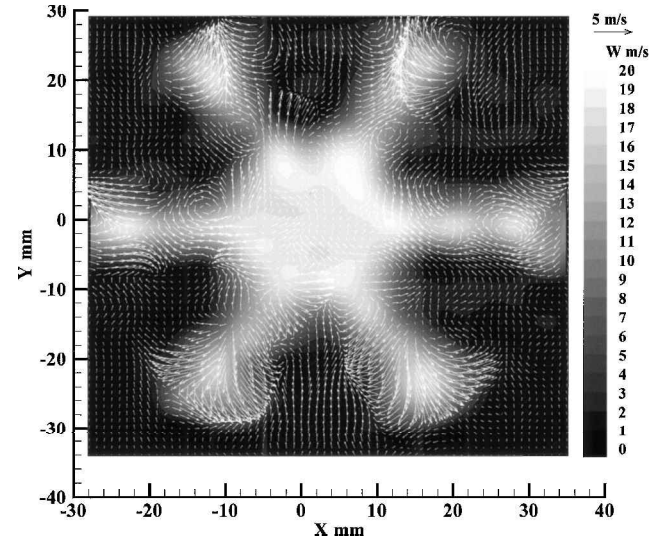

Fig. 4b Instantaneous velocity field with the central scale of 16 mm in the cross plane of $z/D = 0.5$.

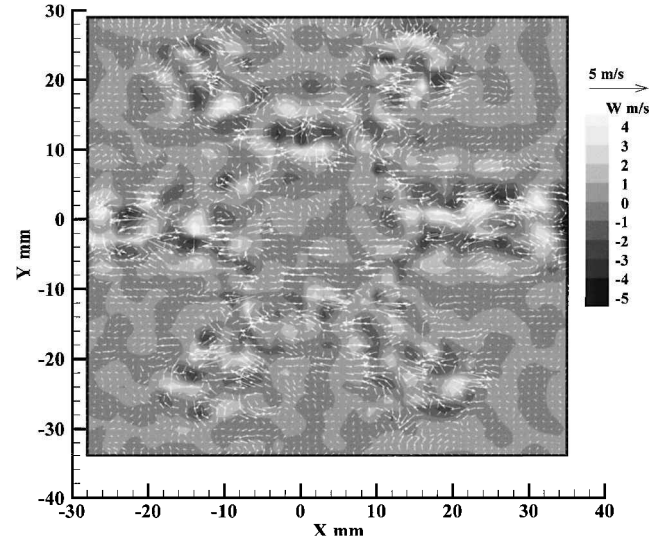

Fig. 4c Instantaneous velocity field with the central scale of 6 mm in the cross plane of $z/D = 0.5$.

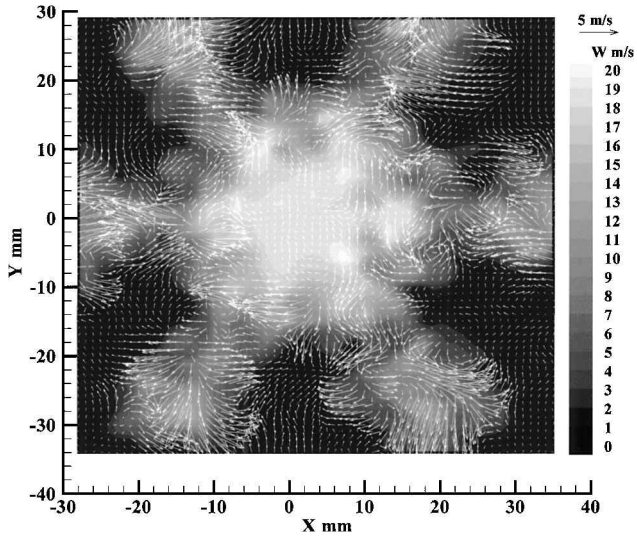

Fig. 5a Instantaneous velocity field of the stereoscopic PIV measurement results in the cross plane of $z/D = 1$.

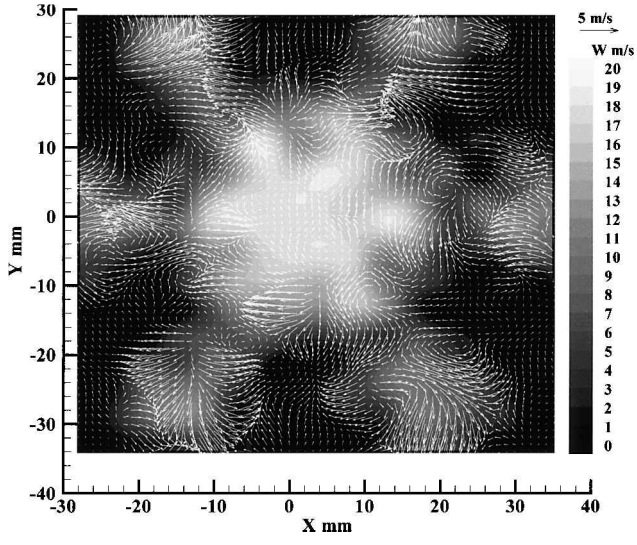

Fig. 5b Instantaneous velocity field with the central scale of 16 mm in the cross plane of $z/D = 1$.

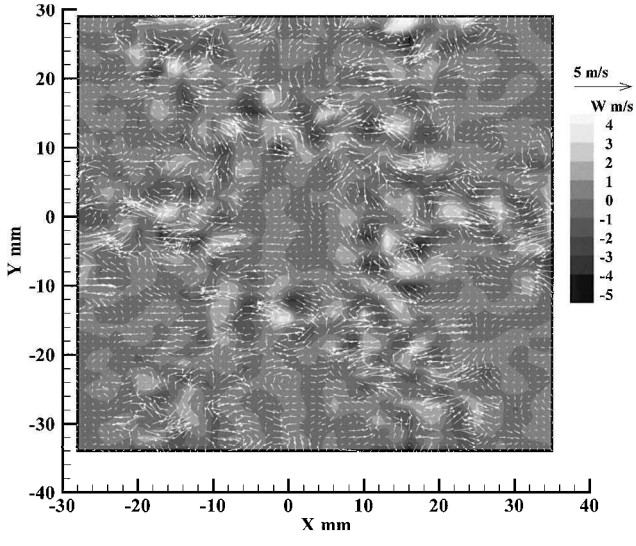

Fig. 5c Instantaneous velocity field with the central scale of 6 mm in the cross plane of $z/D = 1$.

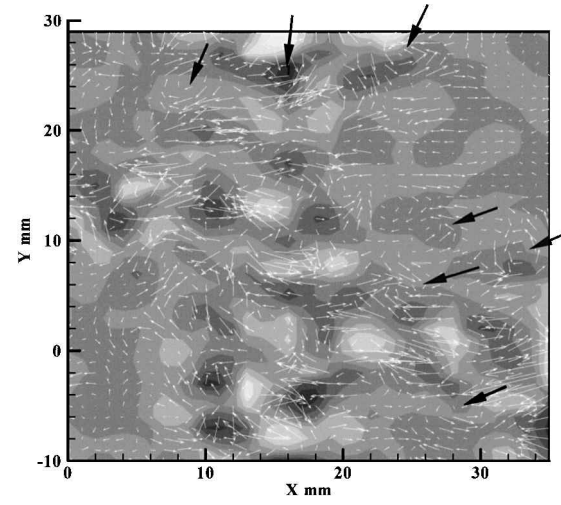

Fig. 5d Zoomed view of instantaneous velocity field at two locations of lobes with the central scale of 6 mm in the cross plane of $z/D = 1$. (Arrows show the positions of small-scale vortices.)

were taken but still mostly visible. From the vector plot three new counter-rotating vortex pairs can be clearly seen in the lobe trough regions. Each counter-rotating pair represents the legs from adjacent horseshoe vortex structures. Though the horseshoe vortex structures have been visualized in previous studies,[7,10] this result provides unquestionable evidence of their existence quantitatively. Such new counter-rotating vortex pairs cannot be observed from the original velocity field of Fig. 5a. The contour of velocity shows that the magnitudes of the axial velocity component decreased in the six lobe regions compared to the preceding location. The instantaneous velocity field with a central scale of 6 mm is plotted in Fig. 5c. The zoomed view on instantaneous velocity vectors at two locations of lobes is shown in Fig. 5d. The velocity vector indicates that the small-scale streamwise vortices, such as indicated by arrows in Fig. 5d, have strongly spread outward along the lobes. By comparing the preceding location, the magnitudes of velocity vectors increase in the lobe regions. It is found that some of these small-scale vortices are contained in the streamwise vortices. It suggests that the small-scale vortices obtain the energy from the large-scale structures and enhance the small-scale mixing process around the lobe regions. The contour of the axial velocity component indicates that the alternate positive and negative peaks also spread outward along the lobes. It implies that the Kelvin–Helmholtz or normal vortex ring expends radially outward as it is expected.

The measured instantaneous velocity field of the cross plane at $z/D = 1.5$, as shown in Fig. 6a, exhibits more complex structures than that in the upstream cross plane of $z/D = 1.0$. The instantaneous large-scale velocity field with a central scale of 16 mm is presented in Fig. 6b. The contour of velocity indicates that the axial velocity components have spread outward along the lobes. The velocity vector plot shows that the large-scale streamwise vortices begin to exhibit signs of breakdown and spread outward. The horseshoes vortices disappear and develop to larger-scale vortices. These streamwise vortices can be clearly seen around the position of lobe and perform the significant large-scale turbulent mixing. The larger ambient flow ejects inward can be observed as a result of the presence of these streamwise vortices. Figure 6c shows the flow structures with a central scale of 6 mm. The small-scale streamwise vortices almost distribute in the whole measured flowfield. They are much more active at the position of the trailing-edge geometry of the lobed nozzle. The turbulence appears to become more intense suggesting that the vortex merging process is an unsteady interaction, and the breakdown of the large-scale streamwise vortices is accompanied by a significant increase in turbulent intense and small-scale vortices. The contour of the axial velocity component indicates that the alternate positive and negative peaks decrease. It means the decrease of small-scale spanwise vortices.

At a farther downstream location of $z/D = 4$, the stereoscopic PIV measurement results are shown in Fig. 7a. The geometry of

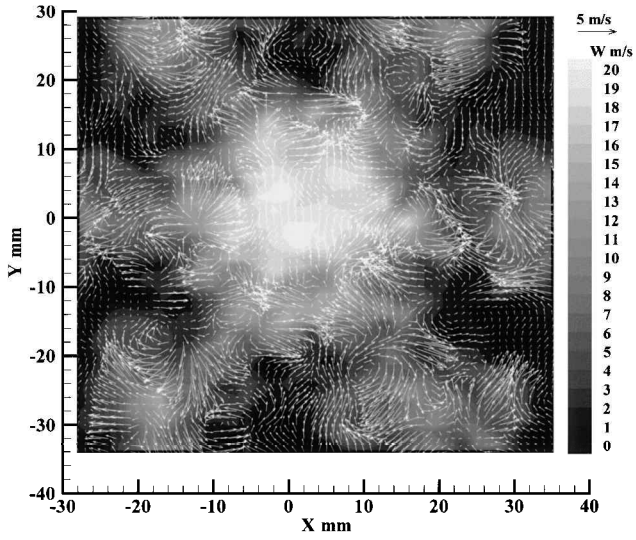

Fig. 6a Instantaneous velocity field of the stereoscopic PIV measurement results in the cross plane of z/D = 1.5.

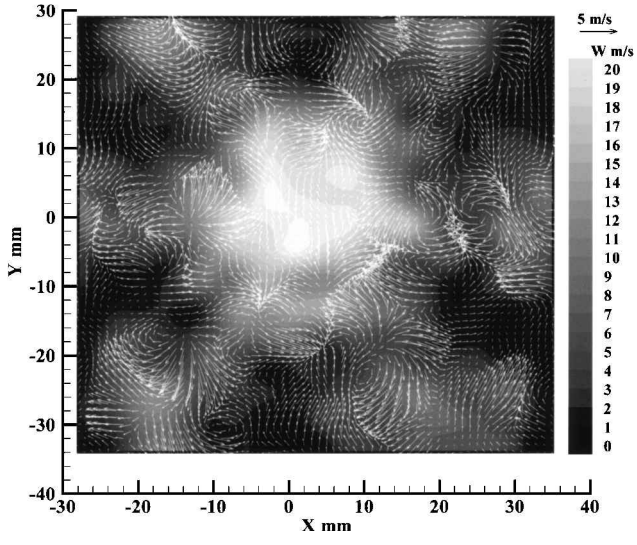

Fig. 6b Instantaneous velocity field with the central scale of 16 mm in the cross plane of z/D = 1.5.

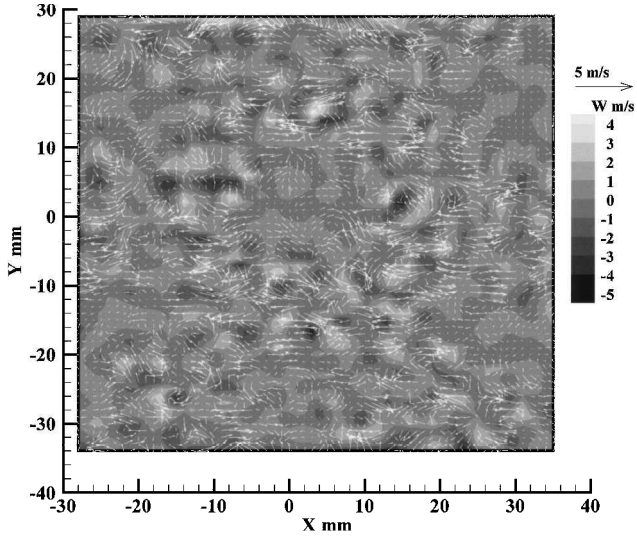

Fig. 6c Instantaneous velocity field with the central scale of 6 mm in the cross plane of z/D = 1.5.

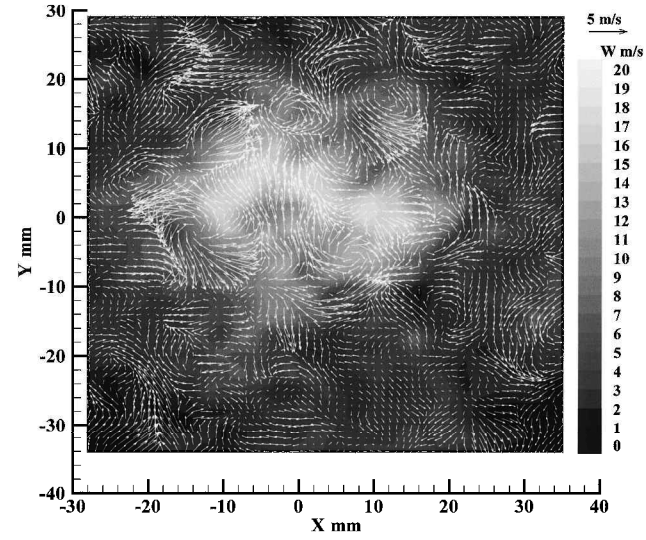

Fig. 7a Instantaneous velocity field of the stereoscopic PIV measurement results in the cross plane of z/D = 4.

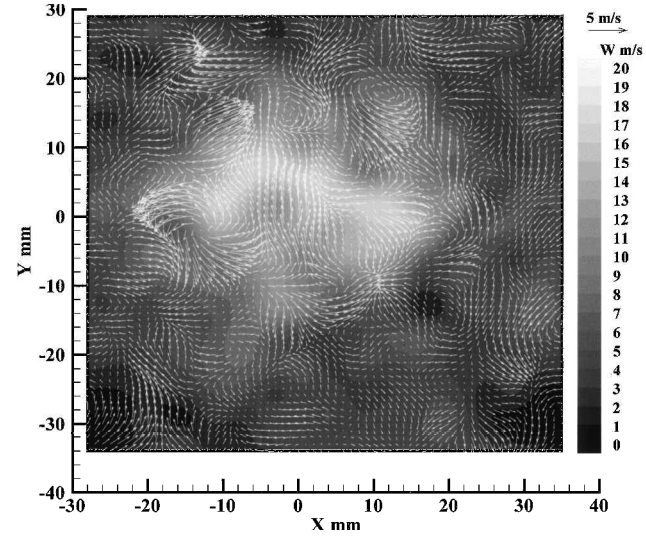

Fig. 7b Instantaneous velocity field with the central scale of 16 mm in the cross plane of z/D = 4.

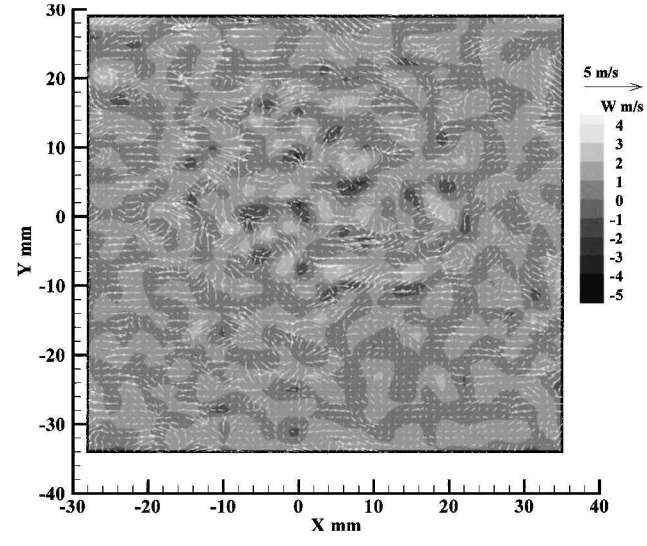

Fig. 7c Instantaneous velocity field with the central scale of 6 mm in the cross plane of z/D = 4.

the lobed nozzle almost cannot be identified from the instantaneous velocity field. The higher magnitude of the axial velocity component is found in the center of the jet flow and decreases rapidly as a result of the intensive mixing of the core jet flow with ambient flow. Figure 7b gives a clear picture of the large-scale structure with a central scale of 16 mm. From the distribution of velocity vectors, the large-scale vortices almost disappear, and the streamwise vortices can be observed in the almost whole measured flowfield. Especially, they are much more active in the jet core region. The velocity field with a central scale of 6 mm is given in Fig. 7c. The velocity vectors indicate that the active streamwise small-scale vortices are distributed in the whole measured flowfield. The contour of the axial velocity component indicates that the alternate positive and negative peaks rapidly decrease and become weak. It implies that the spanwise vortex ring has broken down into many disconnected vortical tubes.

Instantaneous Multiscale Streamwise Vorticity

To study the evolution of multiscale streamwise vortices quantitatively, the instantaneous streamwise vorticity was calculated based on the measured velocity data of the stereoscopic PIV and vector wavelet multiresolution analysis. The normalized instantaneous component of streamwise vorticity $\bar{\omega}_{zi}$ at scale i can be defined in terms of the derivatives of the instantaneous velocity components:

$$\bar{\omega}_{zi} = \frac{D}{U_0}\left(\frac{\partial v_i}{\partial x} - \frac{\partial u_i}{\partial y}\right) \tag{10}$$

where i stands for the scale.

Contours of the measured instantaneous streamwise vorticity at $z/D = 0.5$ are shown in Fig. 8a. The monochrome mappings have been assigned to the vorticity values; the highest concentration is displayed as white and the lowest as black, and the positive and negative vorticity are simultaneously denoted by solid and dashed lines, respectively. The alternative positive and negative peaks can be clearly seen around the lobe edge positions, which indicate the pairs of streamwise vortices. However, it is difficult to identify the smaller-scale vorticity using the measured instantaneous vorticity. Figures 8b and 8c display the distribution of multiscale vorticity in the lobed mixing turbulent jet. The alternative positive and negative vorticities aligned with the lobe, which represent six counter-rotating large-scale streamwise vortex pairs located approximately on either side of the lobe peaks, can be clearly observed in Fig. 8b. These large-scale streamwise vortices, as expected, correspond to vortices appearing in Fig. 8a. Figure 8c shows the distribution of the small-scale vorticity with a central scale of 6 mm. The alternative positive and negative peaks can be clearly seen around the lobe positions, which indicate pairs of the small-scale streamwise vortices.

At $z/D = 1$ the distribution of original instantaneous streamwise vorticity (Fig. 9a) indicates that the six large-scale streamwise vortex pairs break into several smaller vortices. Several new streamwise vortex pairs can be found in the lobe trough regions, which maybe implies the existence of horseshoe vortical structures. Contours of the large-scale vorticity with a central scale of 16 mm, as shown in Fig. 9b, indicate that six counter-rotating large-scale streamwise vortex pairs spread outward along the lobes. The alternative positive and negative vorticity, which represent horseshoe vortices, can be clearly observed in the lobe trough regions. The distribution of the small-scale vorticity with a central scale of 6 mm is presented in Fig. 9c. The stronger alternative positive and negative vorticity is distributed near the lobe positions and lobe trough regions, which indicates more active small-scale streamwise vortex pairs. These small-scale streamwise vortices grow up and strongly spread outward along the lobes compared to the preceding location.

Increasing the downstream distance to $z/D = 1.5$, as shown in Fig. 10a, the distribution of the measured instantaneous streamwise vorticity exhibits many alternative positive and negative peaks. They imply the multiscale of streamwise vortex pairs. The geometry of the lobed nozzle almost cannot be identified. However, Fig. 10b displays only the distribution of large-scale streamwise vorticity. Several pairs of large-scale streamwise vortices can be clearly seen at the position of lobe. The distribution of the small-scale vorticity with a central scale of 6 mm is shown in Fig. 10c. As indicated in the preceding velocity vector plot, many positive and negative peaks that imply the small-scale vortices appear in the whole measured field.

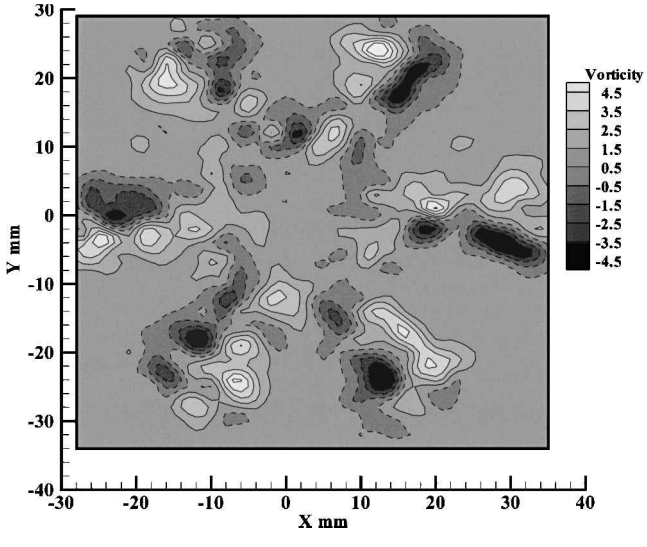

Fig. 8a Instantaneous streamwise vorticity distributions of the stereoscopic PIV measurement results in the cross plane of *z/D* = 0.5.

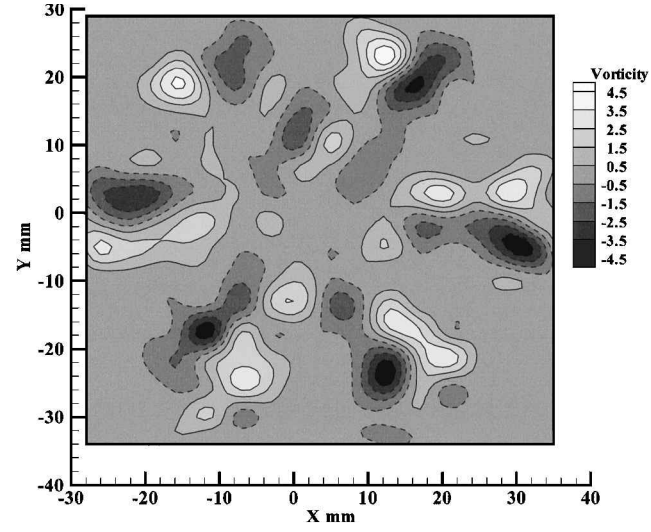

Fig. 8b Instantaneous streamwise vorticity distributions at the central scale of 16 mm in the cross plane of *z/D* = 0.5.

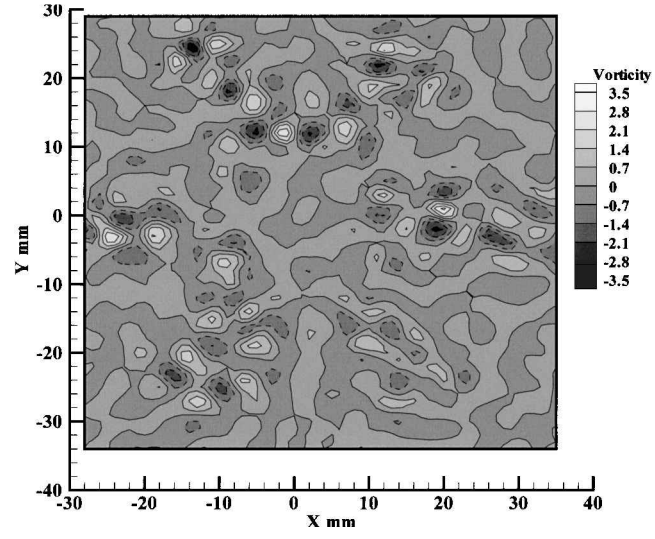

Fig. 8c Instantaneous streamwise vorticity distributions at the central scale of 6 mm in the cross plane of *z/D* = 0.5

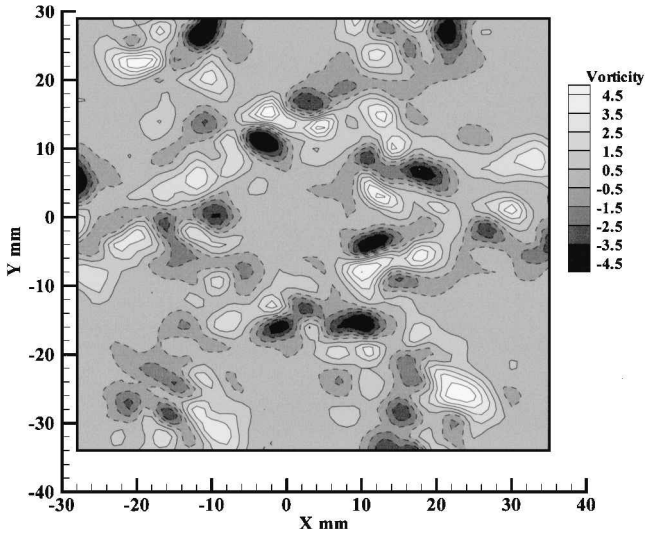

Fig. 9a Instantaneous streamwise vorticity distributions of the stereoscopic PIV measurement results in the cross plane of $z/D = 1$.

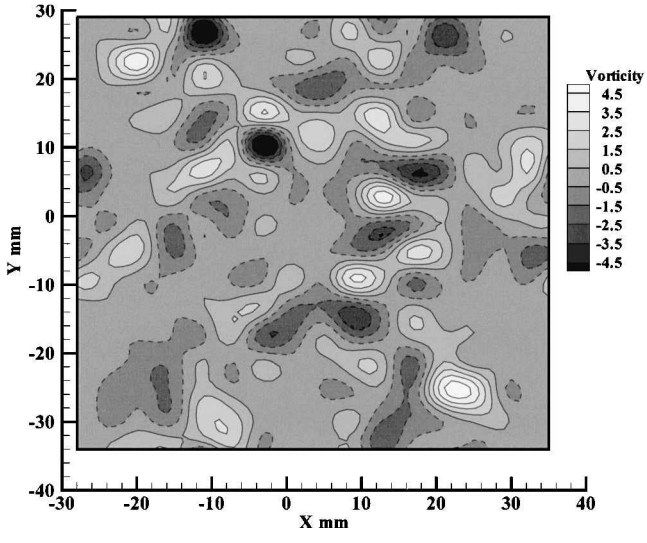

Fig. 9b Instantaneous streamwise vorticity distributions at the central scale of 16 mm in the cross plane of $z/D = 1$.

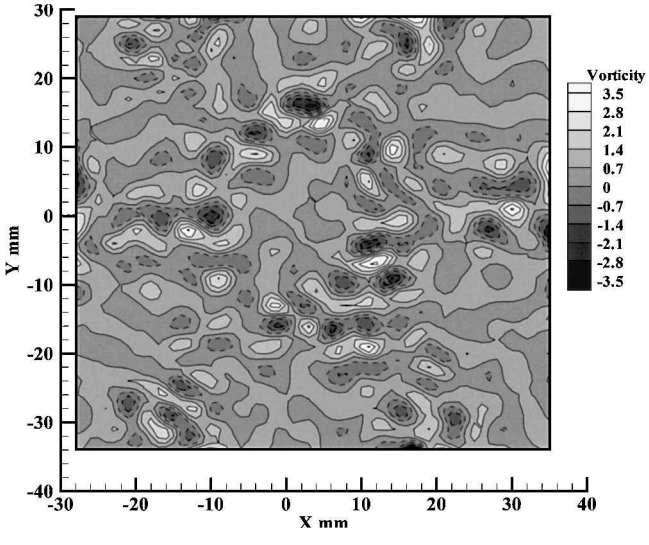

Fig. 9c Instantaneous streamwise vorticity distributions at the central scale of 6 mm in the cross plane of $z/D = 1$.

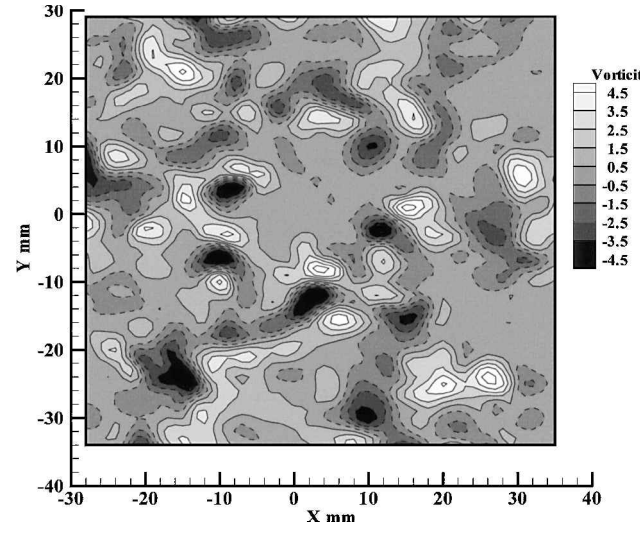

Fig. 10a Instantaneous streamwise vorticity distributions of the stereoscopic PIV measurement results in the cross plane of $z/D = 1.5$.

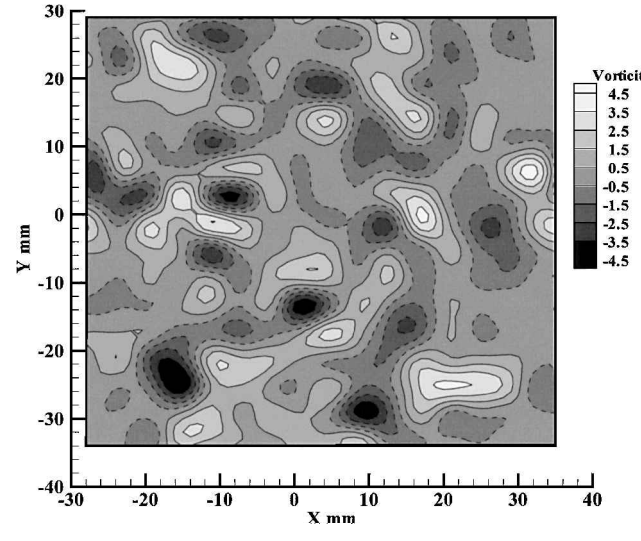

Fig. 10b Instantaneous streamwise vorticity distributions at the central scale of 16 mm in the cross plane of $z/D = 1.5$.

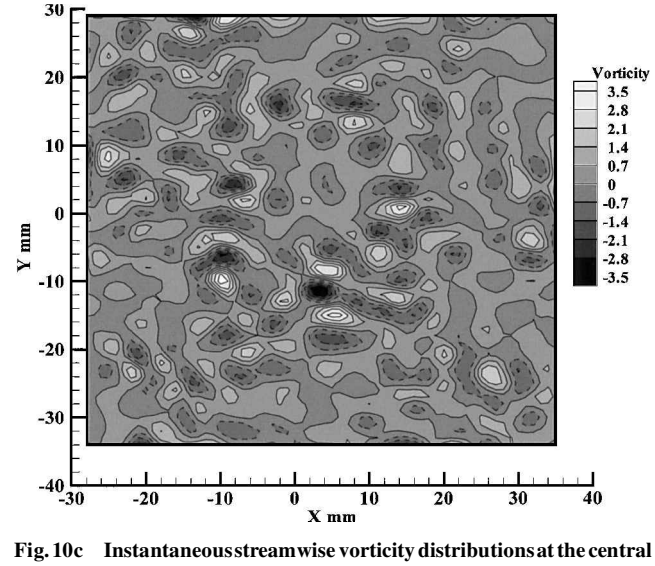

Fig. 10c Instantaneous streamwise vorticity distributions at the central scale of 6 mm in the cross plane of $z/D = 1.5$.

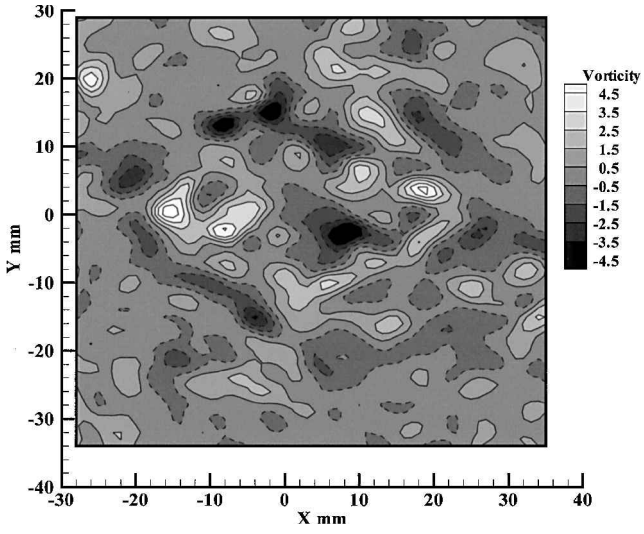

Fig. 11a Instantaneous streamwise vorticity distributions of the stereoscopic PIV measurement results in the cross plane of z/D = 4.

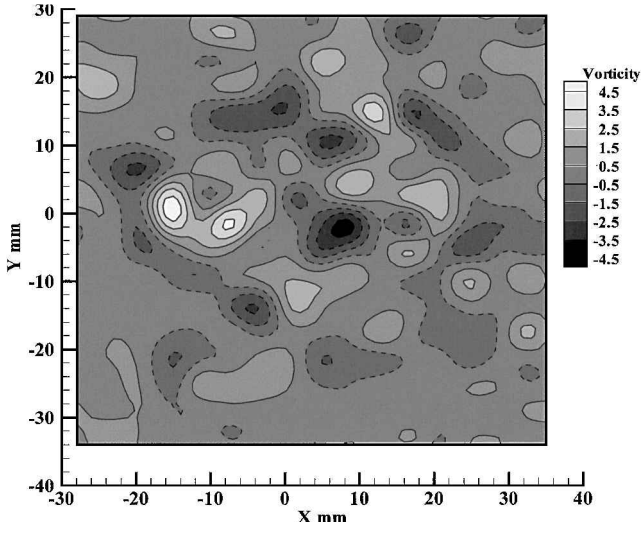

Fig. 11b Instantaneous streamwise vorticity distributions at the central scale of 16 mm in the cross plane of z/D = 4.

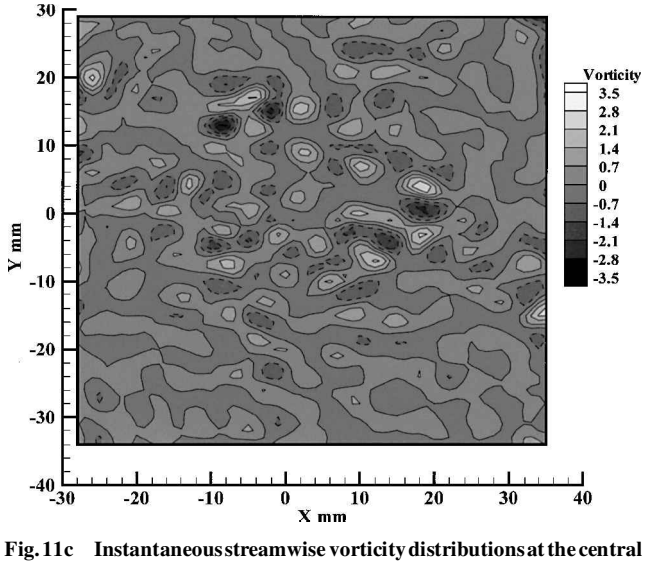

Fig. 11c Instantaneous streamwise vorticity distributions at the central scale of 6 mm in the cross plane of z/D = 4.

At a farther downstream location of $z/D = 4$, from the distribution of the measured instantaneous streamwise vorticity in Fig. 11a many positive and negative peaks mainly distribute in the region of the jet core. The results of the wavelet multiresolution analysis are shown in Figs. 11b and 11c. Both the stronger large-scale and small-scale streamwise vorticity are concentrated in the region of jet core. The maximum vorticity value of these streamwise vortices is found be decreased when compared to that of $z/D = 1.5$.

From the preceding discussion, at different downstream cross planes it can be seen that, as the downstream distance is increased, the size and strength of the large- and small-scale streamwise vortices generated by the lobed nozzle first grow up and appear at the lobe regions. Then they decay and beak up rapidly and can be only observed in the region of jet core.

Conclusions

To reveal the three-dimensional multiscale structure features of the lobed jet mixing flow, vector wavelet multiresolution technique was developed to analyze the three-dimensional measurement results of a high-resolution stereoscopic PIV system in this paper. This technique is unique in its capability to decompose the vector data in both Fourier and physical spaces. The following main results are summarized:

1) The instantaneous three-dimensional velocity vectors were successfully decomposed into large- and small-scale velocity fields based on the wavelet vector multiresolution analysis. It suggests the existence of very strong multiscale turbulent structures in the lobed jet mixing.

2) The large-scale cross-stream flow expands outward along the lobes, and the large-scale ambient flow ejects inward in the lobe troughs.

3) Within the central scale range of 16 mm, the instantaneous pairs of large-scale streamwise vortices and horseshoe vortices can be clearly observed around the lobe peak regions and lobe troughs, respectively, at $z/d = 0.5$ and 1. After $z/d = 1.5$ the large-scale streamwise vortices begin to break down and spread outward.

4) The stronger small-scale streamwise vortices have been confirmed to exist in the lobe regions at $z/d = 0.5$ and 1. These vortices first become intense and spread outward along the lobes and then develop to the whole measured flowfield after $z/d = 1.5$. It indicates that the small-scale streamwise vortices also play a important role in the enhance mixing process.

5) The stronger alternate positive and negative peaks of small-scale axial velocity component are found around the trailing edge of the lobed nozzle at the location of $z/D = 0.5$, 1, and 1.5 within the central scale of 6 mm. These peaks indicate the existence of the Kelvin–Helmholtz or normal vortices.

6) The stronger large- and small-scale streamwise vortices and axial velocity component only appear in the center region of jet at $z/D = 4$.

References

[1]Crouch, R. W., Coughlin, C. L., and Paynter, G. C., "Nozzle Exit Flow Profile Shaping for Jet Noise Reduction," *Journal of Aircraft*, Vol. 14, No. 9, 1977, pp. 860–867.

[2]Paterson, R. W., "Turbofan Mixer Nozzle Flow Field—A Benchmark Experimental Study," *Journal of Engineering for Gas Turbines and Power*, Vol. 106, No. 2, 1984, pp. 692–698.

[3]Werle, M. J., Paterson, R. W., and Presz, W. M., Jr., "Flow Structure in a Periodic Axial Vortex Array," AIAA Paper 87-0610, Jan. 1987.

[4]Eckerle, W. A., Sheibani, H., and Awad, J., "Experimental Measurement of the Vortex Development Downstream of a Lobed Forced Mixer," *Journal of Engineering for Gas Turbines and Power*, Vol. 114, No. 1, 1992, pp. 63–71.

[5]Ukeiley, L., Varghese, M., Glauser, M., and Valentine, D., "Multifractal Analysis of a Lobed Mixer Flowfield Utilizing the Proper Orthogonal Decomposition," *AIAA Journal*, Vol. 30, No. 5, 1992, pp. 1260–1267.

[6]Ukeiley, L., Glauser, M., and Wick, D., "Downstream Evolution of POD Eigenfunctions in a Lobed Mixer," *AIAA Journal*, Vol. 31, No. 8, 1993, pp. 1392–1397.

[7]McCormick, D. C., and Bennett, J. C., Jr., "Vortical and Turbulent Structure of a Lobed Mixer Free Shear Layer," *AIAA Journal*, Vol. 32, No. 9, 1994, pp. 1852–1859.

[8]Belovich, V. M., Samimy, M., and Reeder, M. F., "Dual Stream Axisymmetric Mixing in the Presence of Axial Vorticity," *Journal of Propulsion and Power*, Vol. 12, No. 1, 1996, pp. 178–185.

[9]Belovich, V. M., and Samimy, M., "Mixing Process in a Coaxial Geometry with a Central Lobed Mixing Nozzle," *AIAA Journal*, Vol. 35, No. 5, 1997, pp. 838–84l.

[10]Hu, H., Saga, T., and Kobayashi, T., "Research on the Vortical and Turbulent Structures in the Lobed Jet Flow by Using LIF and PIV," *Measurement Science and Technology*, Vol. 11, No. 6, 2000, pp. 698–711.

[11]Hu, H., Saga, T., Kobayashi, T., and Taniguchi, N., "Stereoscopic PIV Measurement of a Lobed Jet Mixing Flow," *Laser Techniques for Fluid Mechanics*, edited by R. J. Adrian, D. F. G. Durao, M. V. Heitor, M. Maeda, C. Tropea, and J. H. Whitelaw, Springer-Verlag, Berlin, 2002.

[12]Li, H., and Nozaki, T., "Wavelet Analysis for the Plane Turbulent Jet (Analysis of Large Eddy Structure)," *JSME International Journal, Fluids and Thermal Engineering*, Vol. 38, No. 4, 1995, pp. 525–531.

[13]Li, H., "Identification of Coherent Structure in Turbulent Shear Flow with Wavelet Correlation Analysis," *Journal of Fluids Engineering*, Vol. 120, No. 4, 1998, pp. 778–785.

[14]Charles, M., "Analysis of Turbulence in the Orthonormal Wavelet Representation," *Journal of Fluid Mechanics*, Vol. 232, 1991, pp. 469–520.

[15]Staszewski, W. J., Worden, K., and Rees, J. M., "Analysis of Wind Fluctuations Using the Orthogonal Wavelet Transform," *Applied Scientific Research*, Vol. 59, No. 2/3, 1997, pp. 205–218.

[16]Li, H., Takei, M., Ochi, M., Saito, Y., and Horii, K., "Eduction of Unsteady Structure in a Turbulent Jet by Using of Continuous and Discrete Wavelet Transforms," *Transactions of the Japan Society for Aeronautical and Space Sciences*, Vol. 42, No. 138, 2000, pp. 39–44.

[17]Li, H., Takei, M., Ochi, M., Saito, Y., and Horii, K., "Wavelet Multiresolution Analysis Applied to Coherent Structure Eduction of a Turbulent Jet," *Transactions of the Japan Society for Aeronautical and Space Sciences*, Vol. 42, No. 142, 2001, pp. 203–207.

[18]Li, H., Takei, M., Ochi, M., Saito, Y., and Horii, K., "Application of Two-Dimensional Orthogonal Wavelets to Multiresolution Image Analysis of a Turbulent Jet," *Transactions of the Japan Society for Aeronautical and Space Sciences*, Vol. 42, No. 137, 1999, pp. 120–127.

[19]Raffel, M., Willert, C., and Kompenhans, J., *Particle Image Velocimetry*, Springer-Verlag, Berlin, 1998, p. 249.

[20]Hu, H., Saga, T., Kobayashi, T., Taniguchi, N., and Segawa, S., "The Spatial Resolution Improvement of PIV Result by Using Hierarchical Recursive Operation," *Proceedings of the 9th International Symposium on Flow Visualization*, Edinburgh, Scotland, U.K., 2000, Paper 137, pp. 1–12.

W. R. Lempert
Guest Associate Editor